JOURNAL OF PROPULSION AND POWER
Vol. 14, No. 5, September–October 1998

Dynamic Amplification of Fluid Pressure in a Propellant Feed Line

T. V. Nguyen* and W. E. Huffman†
GenCorp Aerojet, Sacramento, California 95813

During the solid rocket booster phase (stage 0) of the Titan IV Space Launch Vehicle K-9 flight, an anomaly occurred in which a burst diaphragm in the stage I oxidizer tank pressurization system ruptured prematurely, resulting in abnormal stage I engine starting conditions. An investigation was conducted and it was found that the most probable cause of the anomaly was oscillatory amplification of the fluid pressure in the pressurization system oxidizer supply line against a volume of trapped gas on the upstream side of the burst diaphragm. This system was driven by liftoff acceleration that induced oscillations in the main oxidizer supply system pressure. A model was formulated to calculate the oscillatory fluid pressure at the burst diaphragm and an experiment was devised to generate data for checking the validity of the model. The experimental setup included a flight-configuration pressurization system oxidizer supply line and a fluid system for inducing pressure oscillations in the liquid column in the line. The pressure of the trapped gas at the burst diaphragm was measured to determine the response to oscillatory fluid pressure imposed at the opposite end of the line. Agreement between the model prediction and experimental results is excellent.

Nomenclature

A = tube cross-sectional area
a_x = vehicle acceleration component along tube length direction
g_x = gravitational acceleration component along tube length direction
L = tube length
n = total number of segments
P_d = driving pressure
P_g = pressure at liquid-gas interface
P_i = initial gas pressure
$P1$ = pressure at tube inlet
$P2$ = pressure at tube outlet
$P3$ = pressure at Freon cylinder outlet
R_{mi} = flow resistance because of hydraulic minor losses
R' = friction-loss factor
V = gas volume
V_i = initial gas volume
v = liquid flow velocity
γ = gas specific heat ratio
ρ = liquid density

Subscript
i = segment number

I. Introduction

THE Titan IV Space Launch Vehicle consists of a two-stage core vehicle powered by GenCorp Aerojet liquid propellant rocket engines with two strap-on solid rocket boosters. Upper stages vary depending on the mission. The stage I and II engines are turbopump-fed and utilize Aerozine 50 as the fuel and nitrogen tetroxide (N_2O_4) as the oxidizer. Ignition of the stage I and then stage II engines occurs at altitude after burnout of the solid rocket boosters.

Vehicle oxidizer tank pressurization during flight is provided by the oxidizer autogenous systems, which are identical in operation for stages I and II. Gaseous N_2O_4 is produced by passing liquid oxidizer through heat exchanger coils in the engine turbine exhaust duct and delivering the gas to the tank top at a controlled flow rate and pressure. The oxidizer supply is tapped off of the oxidizer pump discharge and, at a predetermined pump discharge pressure during engine start, a burst diaphragm in the oxidizer supply line to the heat exchanger ruptures, allowing the flow of liquid to begin. Figure 1 is a schematic diagram of the stage I engine showing the location of the oxidizer autogenous system.

During the flight of Titan IV K-9 an anomaly occurred during the stage 0, or solid rocket booster phase, when the burst diaphragm ruptured at vehicle liftoff from the launch pad rather than at stage I engine start. Flight data showed out-of-family high-pressure oscillations in the engine oxidizer feed system upstream of the burst diaphragm. Although there was no adverse impact to the flight, the anomaly resulted in the flow of liquid N_2O_4 into the gas side of the autogenous system and, therefore, abnormal engine and pressurization system starting conditions, which were outside the Titan flight experience. Analysis showed that the presence of liquid oxidizer in the autogenous line downstream of the burst diaphragm prior to engine ignition will result in a much higher transient pressure in the autogenous line until the liquid is expelled into the tank. The higher pressure significantly increases the risk of rupturing a flexible tube section in the autogenous line.

The premature rupture of the diaphragm was caused by the oscillatory amplification of the pressure of the column of liquid N_2O_4 in the supply line against a volume of nitrogen gas trapped at the upstream side of the burst diaphragm, resulting in pressure peaks above the burst diaphragm rating. This gas bubble is trapped during the filling of the oxidizer system and is present on all flights. This system is driven by the liftoff acceleration at solid rocket booster ignition, which induces engine oxidizer feed system pressure oscillations. Figure 2 shows the configuration of the N_2O_4 supply line and the location of the gas bubble.

Received Sept. 2, 1997; revision received April 20, 1998; accepted for publication May 19, 1998.

*Technical Principal, Thermal and Fluids Department. Member AIAA.

†Project Engineering Specialist, Titan IV Production and Field Support Engineering; currently Senior Project Engineer, National Technical Systems, 11356 Gold Country Boulevard, Gold River, CA 95670.

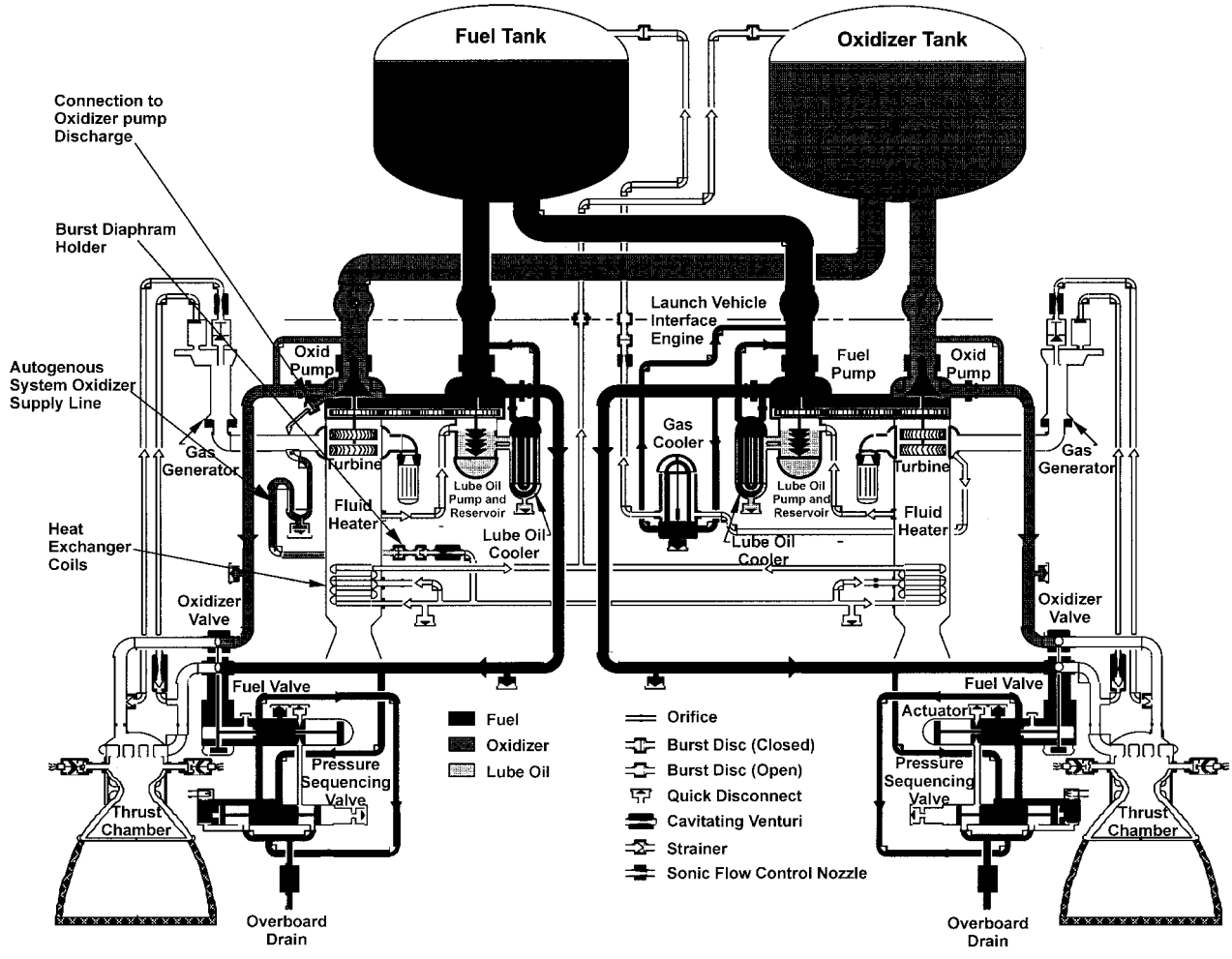

Fig. 1 Titan IV stage 1 engine schematic diagram.

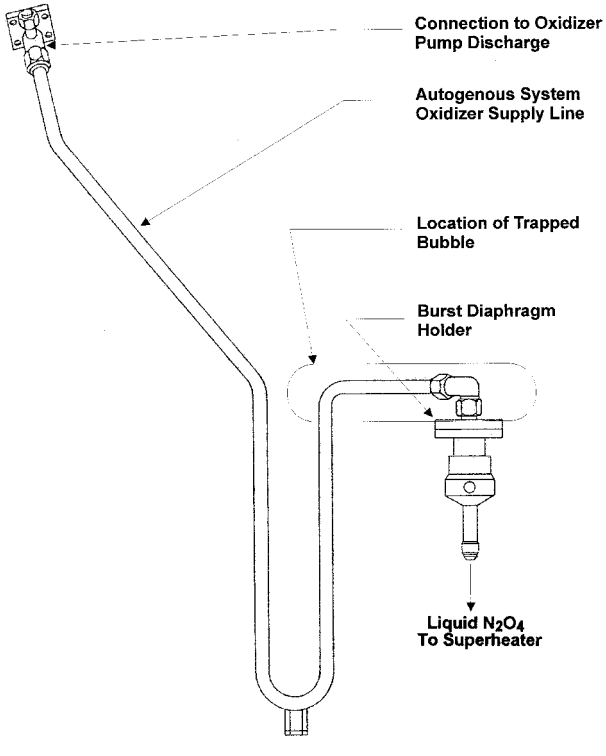

Fig. 2 Autogenous system oxidizer supply line.

A model was formulated to calculate the oscillatory fluid pressure at the burst diaphragm. The model was validated using data from tests conducted at the National Technical Systems (NTS) facility in Fullerton, California.

Subsequent to the K-9 launch, several vehicles were flown with a 0.60-cm (0.237-in.) orifice installed in the oxidizer autogenous line at the connection to the oxidizer pump discharge. The damping provided by this orifice, along with a burst diaphragm with a higher burst pressure rating, provided an interim solution to the pressure oscillation problem. The final solution incorporated a reconfigured oxidizer autogenous line and a liquid-functioned burst diaphragm located at the pump discharge connection. This eliminated the trapped gas bubble and the associated pressure amplification.

II. Model Description

The oxidizer feed system is shown schematically in Fig. 3. The pressure in the main feed line near the inlet to the autogenous line was calculated by Martin Marietta engineers for statistically "worst case" conditions. In the present analysis this pressure was used to drive the fluid system in the autogenous line and the resultant pressure at the burst diaphragm was calculated.

A. Equations

A model was formulated for a fluid system in a line as shown schematically in Fig. 4. The line is filled with liquid with gas trapped at one end. This liquid-gas system is driven by a prescribed pressure at the other end. The line may be composed of any number of tubes having different diameters.

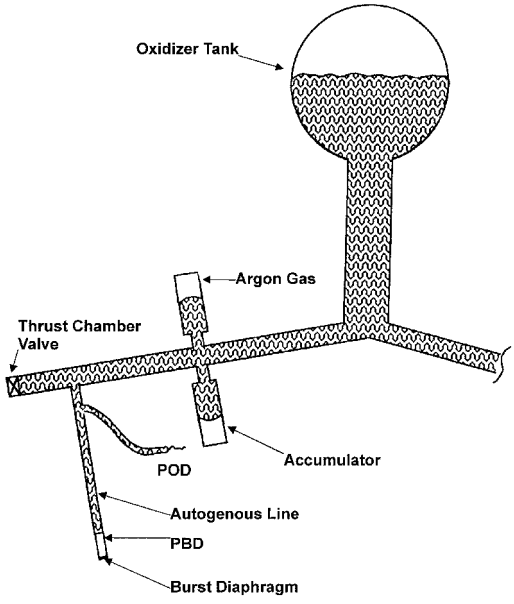

Fig. 3 Oxidizer feed systems.

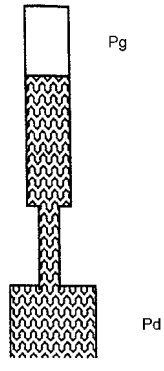

Fig. 4 Modeled fluid systems.

These tubes must be connected in series. Newton's second law was applied to a liquid column in a segment shown in Fig. 5

$$(P_1 - P_2)A - R'|v|v - \rho LAg_x = \rho LA\left(\frac{dv}{dt} + a_x\right) \quad (1)$$

The left-hand side of Eq. (1) is the sum of all forces, including pressure, friction, and body forces. The right-hand side of the equation is the product of liquid mass and acceleration.

Equation (1) can be rearranged as

$$\frac{\rho L}{A}\frac{dQ}{dt} = P_1 - P_2 - R'|Q|Q - \rho L(a_x + g_x) \quad (2)$$

where $Q = Av$ is the volumetric flow rate and $R = R'/A^3$.

The equation has been written in terms of volumetric flow rate Q rather than flow velocity because the former quantity is the same in all line segments at any given time (continuity requirement). This simplifies the mathematical formulation of the problem. Equation (2) is applied to each segment in the line, resulting in a set of equations. Summing this set of equations results in

$$\left(\sum_{i=1}^{n}\frac{\rho L_i}{A_i}\right)\frac{dQ}{dt} = P_d - P_g - \sum_{i=1}^{n}(R_i + R_{mi})|Q|Q - \sum_{i=1}^{n}\rho L_i(a_x + g_x) \quad (3)$$

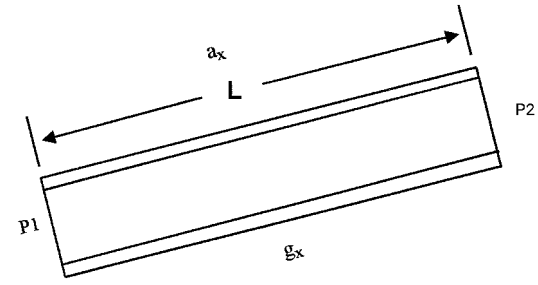

Fig. 5 Various forces acting on a liquid column.

Equation (3) is integrated numerically to calculate instantaneous volumetric flow rate. The volumetric flow rate is then also integrated numerically to calculate the liquid displacement in the last line segment. V is computed from the initial gas volume and the amount of liquid displacement. The instantaneous gas pressure is calculated assuming that the gas compression and expansion are isentropic, i.e.,

$$P_g = P_i(Vi/V)^{\gamma} \quad (4)$$

B. Calculation Procedure

A calculation procedure was developed as follows:

1) Start with known values of pressures, volumetric flow rate, and volumes at a time t. The static equilibrium conditions provide the initial conditions at $t = 0$.

2) Integrate Eq. (3) to obtain the time rate of change of volumetric flow rate at time $t + dt$.

3) Integrate volumetric flow rate to obtain liquid displacement. Calculate the amount of liquid in each of the line segments and the location of the liquid–vapor interface. These calculated parameters were needed to update the values of liquid inertia and flow resistance used in Eq. (3).

4) Compute instantaneous gas volume using the liquid displacement calculated in step 3.

5) Calculate gas pressure Pg using Eq. (4).

6) Increment t by dt and repeat steps 2–6.

Equation (3) was integrated using a predictor–corrector integration scheme. This integration scheme was tested to ensure that no numerical damping was introduced into the solution. The time step was chosen to be small enough that further time step reduction does not change the solution. For all calculations presented in the following sections, the time step used was 0.0001 s.

A computer program was written, using the previously described model, to calculate the instantaneous pressure P_g. Input to the code includes tube lengths, diameters and roughness, liquid density and viscosity, gas specific heat ratio, and driving pressure. The flow resistance caused by friction is calculated internally using the Moody friction factor correlation.[1] The flow resistance because of sudden area changes is also computed internally by the program using a standard minor loss correlation.[1]

III. Test Description

An experiment was devised to generate data for checking the validity of the analytical model. The experimental setup consisted of a flight-configuration stage I oxidizer autogenous supply line, including the engine oxidizer pump discharge attachment fitting and burst diaphragm holder, a hydraulically driven actuator used to induce pressure oscillations into the test fluid and a control system for inputting the required flight pressure profile to the hydraulic actuator. A schematic diagram of the setup is shown in Fig. 6.

Because of the hazards associated with the use of N_2O_4 as the test fluid, an alternate fluid was required. Trial runs were made using water, a desirable alternate because of its availa-

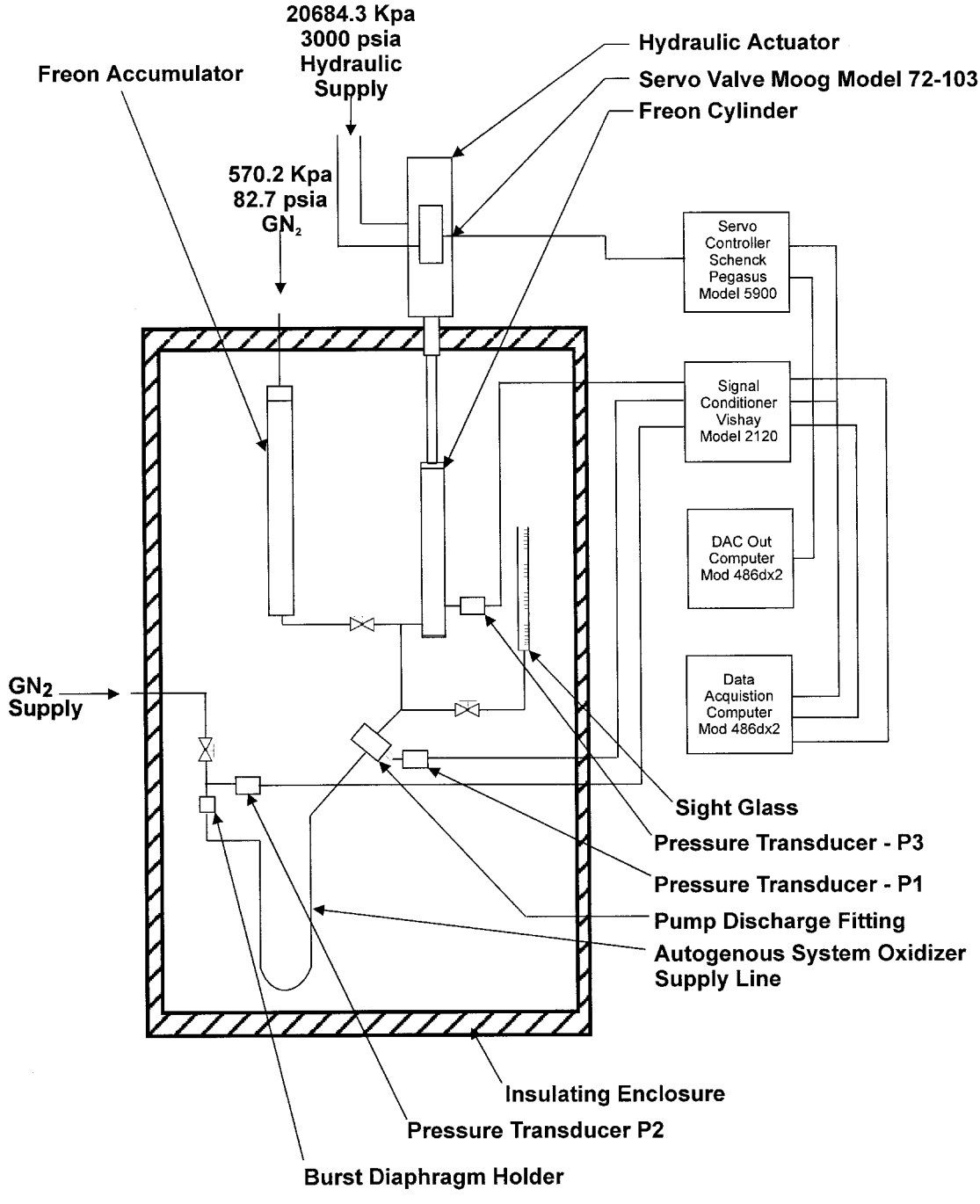

Fig. 6 Schematic diagram of NTS test setup.

bility and ease of handling, but it was found that Freon 11 was a better simulant, because its physical properties are similar to those of N_2O_4 and test results therefore correlate closely with flight data. To compensate for the low boiling point of Freon 11, an insulating box was constructed around the setup, other than the control and hydraulic systems, to maintain test hardware temperature at 18°C (65°F) maximum. This eliminated errors in test results caused by boiling of the test fluid.

The control system shown in Fig. 6 consisted of a digital-to-analog converter (DAC) out computer into which the flight pressure profile was programmed, a signal conditioner for the three instrumentation channels, a data acquisition computer, a digital hydraulic servo-controller and a hydraulic servovalve. The DAC out and data acquisition computers contained the Labtech Notebook 7.0 for DOS data acquisition and control software program and Lotus 123 rev. 2.4 for DOS spread sheet program. The servocontroller was set up to utilize pressure feedback from the transducer at the inlet to the test line ($P1$). This is the point at which the flight pressure data was acquired. $P1$ along with the pressure at the burst diaphragm holder ($P2$) and Freon cylinder ($P3$) were captured by the data acquisition computer during each test run for subsequent printouts.

The Freon system was filled and bled prior to each test run using fluid from an accumulator. With the system pressurized to 570.2 kPa (82.7 psia), a nitrogen bubble was introduced at the burst diaphragm holder to simulate flight conditions. The desired bubble volume, and therefore length, was obtained by displacing an equivalent volume of liquid from the system as measured on a sight glass. The system pressure was maintained at 570.2 kPa (82.7 psia), because this was the pressure at the inlet end of the autogenous system supply line at liftoff of the K-9 vehicle.

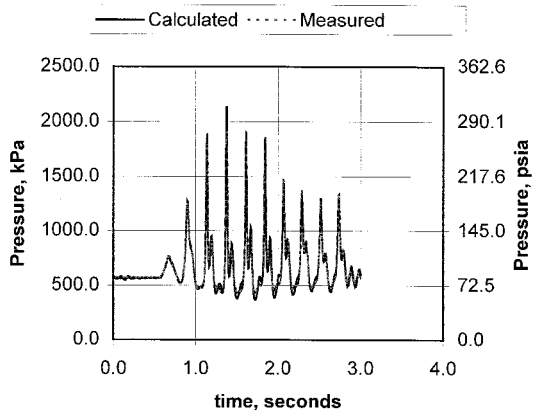

Fig. 7 Comparison between calculated and measured pressure *P*2 for test WN6T1 (bubble size 6.0 in., no orifice).

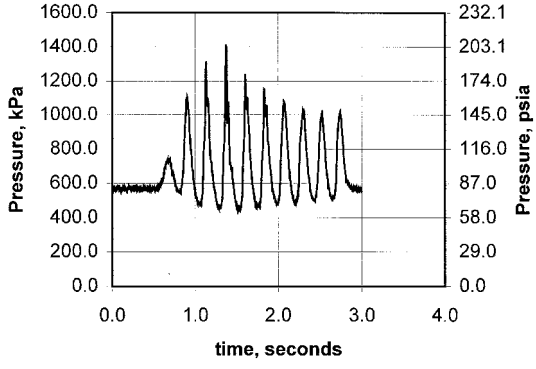

Fig. 8 Driving pressure *P*3 measured in test WN6T1.

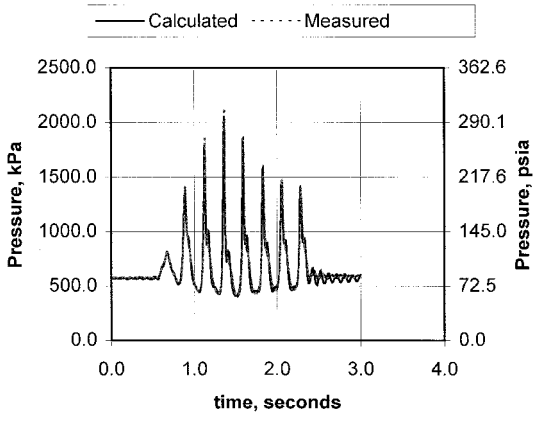

Fig. 9 Comparison between calculated and measured *P*2 for test W26T1 (bubble size 6.0 in., with an orifice of 0.233 in. diameter).

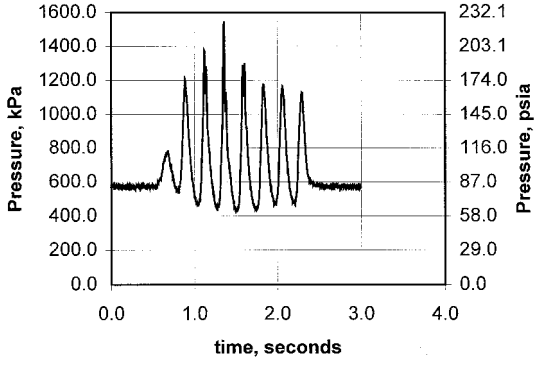

Fig. 10 Driving pressure *P*3 measured in test W26T1.

IV. Model Validation

Calculations were made for a number of tests conducted at National Technical Systems. It should be noted that the test setup has more connectors and flow turns and, hence, a higher resistance than the actual flight hardware. The higher resistance reduces the magnitude of the pressure *P*2. Therefore, test results cannot be directly used to infer the pressure at the burst diaphragm. They are, however, valuable for validating the present model, which is used to calculate the pressure at the burst diaphragm.

Figure 7 shows a comparison between calculated pressure *P*2 and measured data for tests WN6T1 with a gas bubble size of 15.2 (6.0 in.), respectively. The driving pressure *P*3 is shown in Fig. 8. Agreement between calculated results and test data is excellent. It should be mentioned that no orifices were installed in this test.

Figure 9 shows a comparison between calculated pressure *P*2 and measured data from test W26T2, for which an orifice having a diameter of 0.59 cm (0.233 in.) was installed in the line adjacent to the point at which *P*1 is measured. Figure 10 shows the driving pressure *P*3 of this test. Again, agreement between model calculation and test data is excellent.

The orifice was intended to increase resistance, providing more damping to the pressure oscillation. For the flight system the resistance is very low without an orifice and it increases drastically with an orifice. Subsequent to the K-9 launch, an orifice having a 0.60 cm (0.237 in.) diameter was installed in several vehicles in the autogenous line at the connection to the pump discharge. For the test configuration, because of the extra fittings, the resistance is high even without an orifice. Thus, the effect of the orifice is not so pronounced in the test configuration.

V. Calculation of Pressure at Burst Diaphragm

The model was used to calculate the pressure at the burst diaphragm of the K-9 flight. The flight data measured by a pressure transducer located at the pump discharge was used to drive the system. The bubble size was calculated by assuming that during propellant prefill the gas trapped between the pump discharge and the burst diaphragm is compressed from the initial pressure of 101.3 kPa (14.7 psia) to the final pressure of 599.8 kPa (87 psia) and that the compression process is isothermal. The bubble size was calculated to be approximately 20.8 cm (8.2 in.). The peak pressure at the burst diaphragm was calculated to be approximately 2116.7 kPa (307 psia), which is close to the 2068.4 kPa (300 psi) rated pressure of the diaphragm. Calculation also shows that the value of pressure at the burst diaphragm will be even higher with larger bubble size. For example, the pressure was calculated to be approximately 2516.6 kPa (365 psia) for an initial bubble size of 22.9 cm (9.0 in.). The calculations suggested that dynamic amplification of fluid pressure played a major role in causing the premature rupture of the burst diaphragm during the stage 0 operation of the K-9 flight.

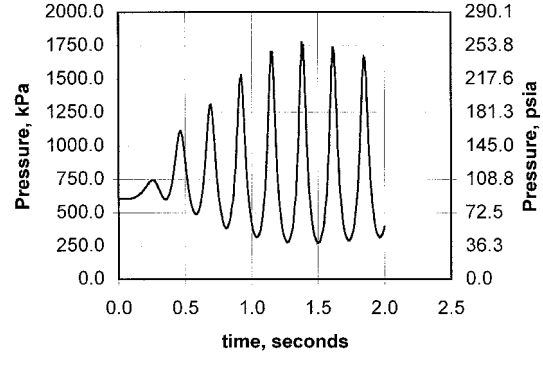

Fig. 11 Worst-case driving pressure POD.

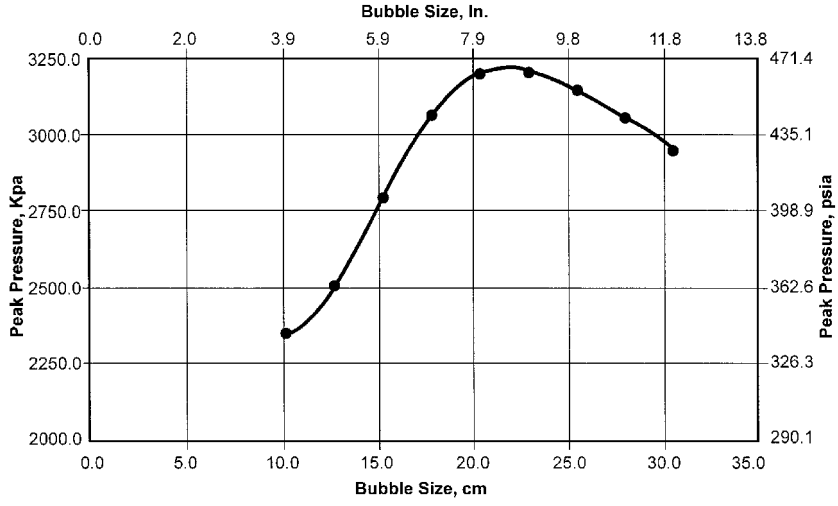

Fig. 12 Peak pressure at burst diaphragm.

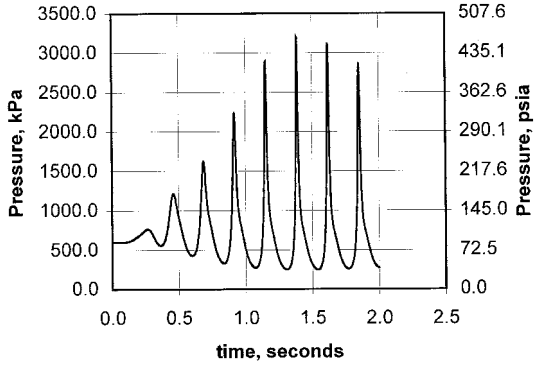

Fig. 13 Calculated pressure at the burst diaphragm under flight worst case conditions (bubble size 9.0 in.).

The model was also used to predict the pressure at the burst diaphragm under "worst-case" driving pressure, which was predicted by Martin Marietta engineers and is shown in Fig. 11. Calculations were made for a configuration that includes an orifice having a diameter of 0.60 cm (0.237 in.), with different gas bubble sizes at the burst diaphragm. As discussed previously the orifice provides additional damping and thus reduces the peak pressure. Figure 12 shows a plot of peak pressure vs gas bubble size. The peak pressure is highest (in resonance with the driving pressure), when the bubble size is 22.9 cm (9.0 in.). A detailed plot of calculated pressure vs time is shown in Fig. 13 for the case where the bubble size is 22.9 cm (9.0 in.). The maximum pressure at the burst diaphragm under worst-case conditions was predicted to be approximately 3206.1 kPa (465 psia), which is below the rated pressure [3240.5–3654.2 kPa (470–530 psi)] of the diaphragm installed on flights subsequent to the flight K-9. Therefore, premature rupture of the diaphragm during stage 0 operation is not expected on future flights. The calculated maximum pressure at the burst diaphragm is conservative because a combination of worst-case oxidizer pump discharge (POD) driving pressure and worst-case bubble size was used in the calculation.

VI. Summary

A model was formulated to calculate instantaneous pressure in a fluid line filled with liquid but having gas trapped at one end, under the influence of a prescribed pressure at the other end.

The model was validated using data from several tests conducted at NTS. Agreement between model prediction and test data is excellent.

Calculations using the model suggested that dynamic amplification of fluid pressure played a major role in causing the premature rupture of the burst diaphragm during the stage 0 operation of the K-9 flight.

The model was applied to calculate the pressure at the burst diaphragm under the worst-case driving pressure provided by Martin Marietta. The peak pressure at the burst diaphragm was calculated to be approximately 3206.1 kPa (465 psia), less than the rated pressure of the new diaphragm. Therefore, premature rupture of the new diaphragm is not expected.

Acknowledgment

Presented as Paper 1.9 at the 3rd International Symposium on Space Propulsion, Beijing, People's Republic of China, Aug. 11–13, 1997.

Reference

[1]"Flow of Fluids Through Valves, Fittings, and Pipes," Crane Technical Paper 410, 1976.